Effect of Anions on the Photocatalytic Activity of Fe(III) Salts Impregnated TiO_2

Praveen K. Surolia, Rajesh J. Tayade, and Raksh V. Jasra*

Discipline of Inorganic Materials and Catalysis, Central Salt and Marine Chemicals Research Institute, Bhavnagar-364 002, India

This present work focuses on the photocatalytic activity of Fe(III) salt-impregnated TiO_2 catalysts for studying the effect of anion on the photocatalytic activity of the salt-impregnated catalysts. The salt-impregnated TiO_2 photocatalyst samples prepared using $FeCl_3$, $Fe(NO_3)_3$, and $Fe_2(SO_4)_3$ were characterized by X-ray diffraction (XRD), UV−vis diffuse reflectance spectrophotometry (DRS), Fourier transform infrared absorption spectrophotometry (FT-IR), and surface area measurement by N_2 adsorption. Fe(III) ion impregnation of TiO_2 with different salts is observed to influence photocatalytic degradation of acetophenone. Fe(III) salt anions were observed to influence the initial rate of degradation. For example, the initial rate of degradation of acetophenone decreases with an increase in percentage of Fe(III) ions in the case of the catalysts prepared using ferric nitrate and ferric chloride salts. However, the initial rate of degradation was observed to increase with ferric sulfate impregnated catalysts. The final percentage degradation of acetophenone was found to increase continuously with an increase in Fe(III) ion concentration, irrespective of the anion. These observations have been discussed in terms of influence of the presence of Fe(III) ions on the recombination of the electron and holes generated during UV irradiation of TiO_2. Similarly, the effect of anion has been discussed in terms of radical-scavenging ability of chloride and radical-generating ability of sulfate anions.

Introduction

In the last decade, research efforts have been directed to enhance the activity of the photocatalysts using various methods such as increasing catalyst surface-to-volume ratio, sensitization of the catalyst using dye molecules,[1,2] doping the catalyst with nonmetals such as nitrogen, carbon, and sulfur and catalyst impregnation of metal ions.[3−6] It has been demonstrated that the addition of a low percentage of a metal ion such as Pt, Ag, Au, Cu, Ni, Co, Fe, and Mg in TiO_2 improves[7−9] its photocatalytic activity. Fe metal ions impregnation has been studied for photocatalytic efficiency enhancement of the TiO_2 catalysts, and varied results are reported.[10−13] This could be due to the different synthesis methods, the percentage of ion impregnated, and the source used for the impregnation of Fe. For example, Choi et al.[10] suggested that the ability of a dopant to function as an effective electron-hole trap is related to the dopant concentration and reported the highest activity at 0.5 at. % of Fe(III). Li et al.[11] studied the photocatalytic oxidation of cyclohexane and found higher photocatalytic activity with Fe(III) ion impregnation. Vamathevan et al.[12] found lower activity of catalyst with 5 atomic % or higher loading of Fe(III) in TiO_2 particles for the degradation of sucrose. These studies concluded that an increasing amount of iron could cause its agglomeration at the surface of TiO_2 to form α-Fe_2O_3. This results in the reduction of catalytically active and electron relay sites and thereby negatively influences the photocatalytic activity. The present work was carried out to specifically study the effect of the anion of Fe(III) salts used for impregnation on the photocatalytic activity of P25 Degussa TiO_2 photocatalyst. To study the photocatalytic activity, degradation of acetophenone in aqueous medium was used as a model organic compound with ultraviolet irradiation.

Experimental Section

Materials. Titanium dioxide (P25) was purchased from Degussa Corporation (Degussa AG, Frankfurt, Germany). Ferric nitrate, ferric sulfate, and ferric chloride were procured from s. d. Fine Chem. Ltd., Mumbai, India. Acetophenone, analytical reagent (AR) grade, was purchased from E. Merck, India. Deionized distilled water was used to make up the reaction mixture.

Catalysts Preparation. Catalysts were prepared by wet impregnation method. P25 Degussa TiO_2 was suspended in aqueous solutions of the Fe(III) salt. The mixture was stirred for 36 h under normal room conditions to get the loading of Fe metal ion of 0.1, 0.5, 1.0, 5.0, and 10.0% (w/w) followed by drying of the slurry under vacuum using rotavapor and further drying in an oven at 353 K for 12 h. The thus-dried catalysts were thoroughly ground with an agate mortar pestle and calcined at 723 K temperature for 4 h in the presence of air. The impregnated TiO_2 catalysts with ferric nitrate were denoted as Ti−N1, Ti−N2, Ti−N3, Ti−N4, and Ti−N5, wherein the numeral denotes the percentage (w/w) of iron as 0.1, 0.5, 1.0, 5.0, and 10.0, respectively. Similarly for Fe, impregnated catalysts using ferric chloride and ferric sulfate were denoted as Ti−C1, Ti−C2, Ti−C3, Ti−C4, Ti−C5, Ti−S1, Ti−S2, Ti−S3, Ti−S4, and Ti−S5, respectively. The actual loading of Fe(III) ion was confirmed by inductively coupled plasma (ICP)−optical emission spectrophotometer analysis, and values are given in Table 3.

Catalyst Characterization. The catalysts were characterized by powder X-ray diffraction (XRD) recorded at 295 K using Phillips X'pert MPD system with Cu Kα_1 radiation (λ = 0.15405 nm). Diffraction patterns were measured in 2θ range from 10°−60° at a scan speed of 0.1° s^{-1}. The XRD peaks of crystal plane 101 for anatase appeared at 25.3 (2θ) and at 27.4 (2θ) for 110 plane of rutile. These peaks were selected to determine the percentage of anatase and rutile phases[14] in the TiO_2 sample. The percentage of anatase, A (%), was determined using the following equation,

$$A\ (\%) = 100/(1 + 1.265 I_R/I_A) \quad (1)$$

where I_R is the intensity of the rutile peak at $2\theta = 27.4$ and I_A is the intensity of the anatase peak at $2\theta = 25.3$. The crystallite

* To whom correspondence should be addressed. E-mail: rvjasra@csmcri.org. Tel.: +91 278 2471793. Fax: +91 278 2567562.

10.1021/ie0702678 CCC: $37.00
Published on Web 08/16/2007

Table 1. XRD Data of the Catalysts

catalyst	crystallite size[a] (nm)	anatase (%)	rutile (%)	crystallinity[b] (%)	lattice constants (Å) $a = b$	lattice constants (Å) c
P-25	25	80	20	100	3.7830	9.4940
Ti−N1	22	78	22	84	3.7811	9.4936
Ti−N2	22	78	22	85	3.7804	9.4880
Ti−N3	22	78	22	83	3.7802	9.4877
Ti−N4	22	79	21	78	3.7793	9.4850
Ti−N5	22	78	22	66	3.7787	9.4850
Ti−C1	23	78	20	86	3.7817	9.4920
Ti−C2	23	78	22	85	3.7797	9.4887
Ti−C3	22	78	22	84	3.7797	9.4885
Ti−C4	22	78	22	79	3.7787	9.4813
Ti−C5	22	78	22	67	3.7785	9.4812
Ti−S1	22	78	22	82	3.7810	9.4894
Ti−S2	22	78	22	81	3.7808	9.4893
Ti−S3	22	78	22	80	3.7807	9.4892
Ti−S4	22	78	22	57	3.7807	9.4890
Ti−S5	21	78	22	39	3.7806	9.4888

[a] Calculated at $2\theta = 25.3$, the most intense peak. [b] Calculated by measuring the total peak area under five major peaks at $2\theta = 25.3$, 37.7, 47.9, 53.9, and 55.1.

Table 2. Textural, Electronic, and Photocatalytic Properties of Synthesized Catalysts

catalyst	surface area (m^2/g)	band gap (eV)	color	initial rate ($\times 10^6$ mol·min^{-1})	rate constant (k) ($\times 10^{-2}$ min^{-1})
P-25	50	3.17	white	8.00	2.64
Ti−N1	47	3.17	white	8.33	2.88
Ti−N2	49	3.17	white	6.93	2.25
Ti−N3	47	3.17	brown	6.33	2.21
Ti−N4	46	3.17, 2.13	red−brown	5.80	2.19
Ti−N5	47	3.17, 2.13	red−brown	5.66	2.17
Ti−C1	50	3.17	white	7.13	2.19
Ti−C2	48	3.17	white	6.80	2.07
Ti−C3	48	3.17	brown	6.40	2.07
Ti−C4	44	3.17, 2.13	red−brown	6.33	2.07
Ti−C5	43	3.17, 2.13	red−brown	6.13	2.07
Ti−S1	48	3.17	white	6.06	1.95
Ti−S2	50	3.17	white	7.46	2.56
Ti−S3	48	3.17	white	7.73	2.61
Ti−S4	24	3.17, 2.84	pale-yellow	8.00	2.64
Ti−S5	15	3.17, 2.84	pale-yellow	8.20	2.64

Table 3. ICP Analysis Results of the Prepared Samples

catalyst	% Fe from ICP	catalyst	% Fe from ICP	catalyst	% Fe from ICP
Ti−N1	0.13	Ti−C1	0.13	Ti−S1	0.11
Ti−N2	0.47	Ti−C2	0.52	Ti−S2	0.55
Ti−N3	1.21	Ti−C3	1.12	Ti−S3	0.98
Ti−N4	5.13	Ti−C4	5.05	Ti−S4	4.95
Ti−N5	9.87	Ti−C5	10.11	Ti−S5	10.07

size of TiO_2 was determined from the characteristic peak of $2\theta = 25.3$ (101) for anatase and $2\theta = 27.4$ (110) for rutile using the Scherrer formula,[15] with a shape factor (K) of 0.9

$$\text{crystallite size} = K\lambda/W\cos\theta \tag{2}$$

where $W = W_b - W_s$, W_b is the broadened profile width of the experimental sample, W_s is the standard profile width of the reference silicon sample, and λ is the wavelength of X-ray radiation (Cu $K\alpha_1 = 0.15405$ nm). The crystallinity of the catalysts was calculated with reference to P25 Degussa as 100%, by taking the average of five major anatase peaks of the catalyst ($2\theta = 25.3$, 37.7, 47.9, 53.9, and 55.2). The unit cell volumes were calculated by crystal builder module in Cerius^2 v. 4.1 (Accelrys Software, Inc., San Diego, CA).

The band gap energy of the catalysts was determined using the diffuse reflectance spectroscopy (DRS). The spectrophotometer (Shimadzu UV-3101PC) was equipped with an integrating sphere, and $BaSO_4$ was used as a reference.[16,17] The spectra were recorded at room temperature in the wavelength range of 250−800 nm. The band gap energies of catalysts were calculated according to the following equation,

$$\text{band gap (EG)} = hc/\lambda \tag{3}$$

where EG is the band gap energy (eV), h is the Planck's constant, c is the light velocity (m/s), and λ is the wavelength (nm).

The FT-IR spectroscopic measurements were carried out using a Perkin-Elmer GX spectrophotometer. The spectra were recorded in the range 400−4000 cm^{-1} with a resolution of 4 cm^{-1} using a KBr wafer technique.

An inductively coupled plasma−optical emission spectrophotometer (ICP−OES, Optima 2000 DV, Perkin-Elmer, Eden Prarie, MN) was used to determine the percentage of the metal ion present in the degraded solution after performing photocatalytic experiments and for the actual loading of Fe(III) ion in the prepared catalyst samples. The existence of chloride ion was confirmed by a Brucker S4 Pioneer WD XRF instrument.

Specific single point surface areas of catalysts were determined from N_2 adsorption at 77 K by using a volumetric adsorption setup (ASAP 2010, Micromeritics, U.S.A.). The catalysts were degassed under vacuum (10^{-2} Torr) at 623 K for 4 h, prior to adsorption measurement.

Photocatalytic Activity. Photocatalytic degradation of acetophenone was carried out using a reactor consisting of two parts as reported earlier.[9] The first part is the inner quartz double-wall jacket with inlet and outlet for the water circulation to maintain the temperature of the reaction mixture. This jacket has an empty chamber at the center for immersion of the mercury vapor lamp. UV irradiation is done with 125 W mercury vapor lamp (Crompton Greaves Ltd., India). The second part is the outer borosilicate glass container (volume 250 mL after insertion of the inner part) in which the reaction takes place. The magnetic stirrer was kept below the reactor for continuous stirring. The 5 mL reaction mixture was withdrawn from the port by syringe at different time intervals. The pH of the reaction mixture was measured by pH meter prior to reaction. The pH of the reaction mixture was observed in the range of 5.96−6.00. No acid and alkali were added to achieve the pH. It shows that no ion leaching is observed before irradiation, and the reaction mixture shows nearly constant pH.

The photocatalytic activity of the catalysts was evaluated by measuring the decrease in concentration of acetophenone in the reaction solution. Prior to commencing irradiation, a suspension containing 50 mg of the catalyst and 250 mL of aqueous solution of ca. 50 ppm of acetophenone was stirred continuously for 30 min in the dark followed by the collections of the sample and its analysis for acetophenone. Following this, the solution was irradiated and samples were withdrawn for analysis by a syringe from the irradiated suspension at intervals of 10 min for the first 1 h and every hour thereafter. The catalysts were separated by centrifugation from the aqueous solutions prior to analyzing the samples. The concentrations of acetophenone in the solution were determined by UV−visible spectrophotometer (Cary 500, Varian, Palo Alto, CA). The absorbance was measured at $\lambda_{max} = 246$ nm for acetophenone.

Results and Discussion

Structural Properties. Figure 1 shows the XRD patterns of $Fe(NO_3)_3$, $FeCl_3$, and $Fe_2(SO_4)_3$ impregnated catalysts. The 2θ values at 25.3 and 27.4 correspond to anatase and rutile phases,

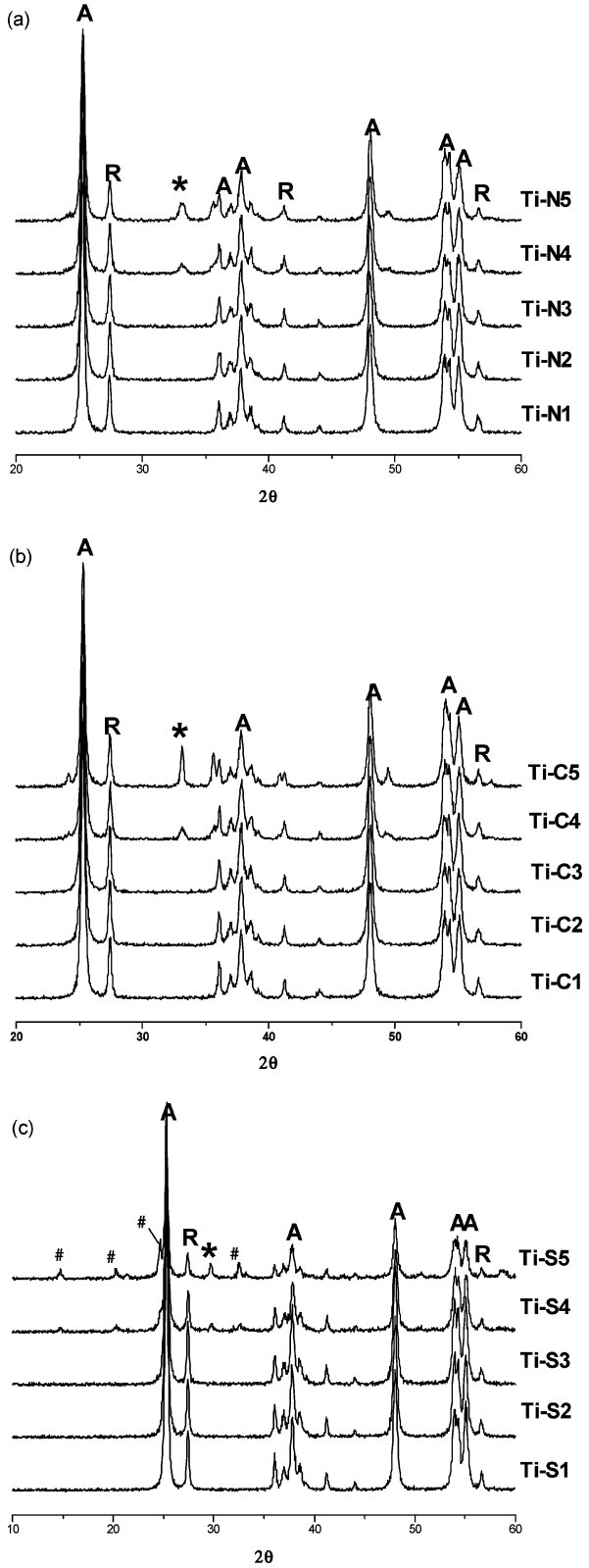

Figure 1. XRD analysis of Fe(III) salts-impregnated TiO_2: (a) Ti−N series, (b) Ti−C series, and (c) Ti− S series. * indicates the α-Fe_2O_3 peak, and # indicates the SO_4^{2-} peak.

respectively. α-Fe_2O_3 shows diffraction at 2θ value of 33.0, whereas the SO_4^{-2} group shows diffraction at 2θ values of 14.75, 20.28, and 24.65. The confirmation of these peaks was done by comparing with the XRD pattern of pure ferric sulfate. The peaks assigned to the Fe(III) were not observed in the XRD pattern of Fe-impregnated TiO_2 samples below 5%. However,

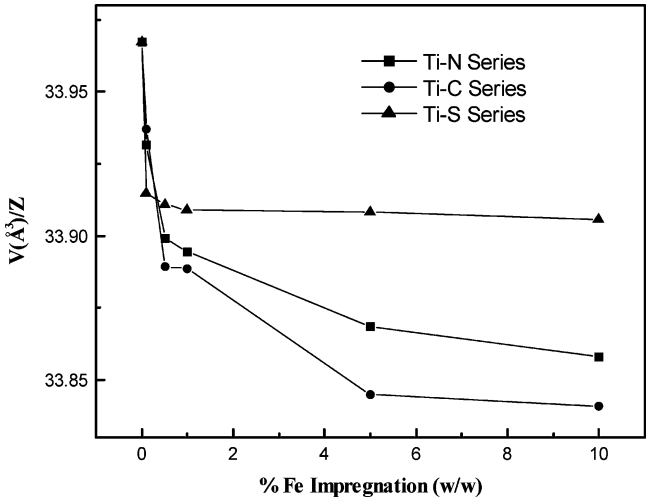

Figure 2. Change of *V*/*Z* with Fe impregnation content, where *V* and *Z* are the unit cell volume and the number of formulas per cell, respectively.

the peak that corresponds to α-Fe_2O_3 was observed in all the Fe(III)-impregnated TiO_2 catalysts with impregnation >5%, indicating its presence on the external surface of the catalysts at higher loadings of Fe(III) ion. XRD analysis showed that the TiO_2 structure is intact after iron salt impregnation. It has been reported[9,18] that, because of the small ionic size of Fe(III) (64 pm) and the low percentage of impregnation, Fe(III) could substitute into the TiO_2 lattice. All the samples have a tetragonal structure with space group $D_{4h}^{19}I41/amd$, and the lattice parameters decrease along all three axes as the Fe(III) content is increased. The lattice constants for the anatase phase of Degussa P25 were calculated as $a = b = 3.7830$ Å and $c = 9.4940$ Å. The theoretical values for the anatase phase of TiO_2 calculated using Cerius[2] software are $a = b = 3.7760$ Å and $c = 9.4860$ Å, and similar values were reported by Diebold[19] with $a = b = 3.782$ Å and $c = 9.502$ Å. The values of the calculated lattice constants of Degussa P25 were found to decrease with an increase in the Fe(III) ion content (Table 1), supporting substitution of Fe(III) ions in the lattice at lower Fe(III) loadings. Figure 2 shows the change of *V*/*Z* with impregnation content, where *V* and *Z* are the cell volume and the number of formulas per cell, respectively. The unit cell volumes were calculated by the crystal builder module in Cerius[2] v. 4.1.[20] These data show that, for a small amount of Fe(III) impregnation, there is a sharp decrease in the *V*/*Z* ratio, supporting substituting of Fe(III) ions in the TiO_2 lattice. Nearly constant or gradual decrease in the *V*/*Z* ratio at higher Fe(III) impregnation also supports the observation that, after a certain impregnation, Fe(III) is residing on the external surface of TiO_2, as also seen from XRD analysis.

It is also seen in Table 1 that there is no decrease in the anatase and rutile phase percentages, but the intensity of all peaks was observed to reduce, which could be attributed to formation of ferric oxide on the surface of TiO_2. A decrease in the percentage crystallinity was observed with an increase in the loading of the Fe(III) ion. This decrease was seen to be higher in the case of the Ti−S series of catalysts and at higher percentage loadings of the Fe(III) ion. The pseudo-brookite peak is not observed, because there is a little tendency for bulk reactions between Fe_2O_3 and TiO_2 up to 823 K.[21]

The FT-IR transmission spectra of the catalysts are shown in Figure 3. The spectra show the Ti−O−Ti stretching band at 400−600 cm^{-1};[22] α-Fe_2O_3 confirmed by XRD spectra also showed the vibrational band at 450−470 cm^{-1} with the TiO_2 vibrational band.[21] The FT-IR spectra of sulfated metal oxide

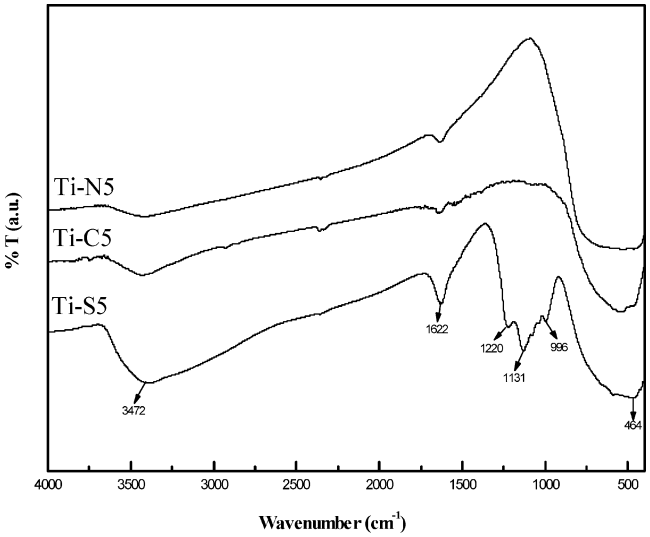

Figure 3. FT-IR spectra of 10% Fe(III) salts-impregnated TiO_2 catalysts using different anionic sources.

show a broad band at 1200−900 cm^{-1}. This is the characteristic frequency of SO_4^{2-}. The observed broad band resulted from the lowering of the symmetry in the free SO_4^{2-} (Td point group). The symmetry of bonded SO_4^{2-} to titania surface can be lowered either C_{3V} or C_{2V} point group. The peaks at 1220−1222, 1131, and 996−997 cm^{-1} are characteristic of inorganic chelating bidentate sulfates, which are assigned to asymmetric and symmetric stretching frequencies of S=O and S−O bond.[23]

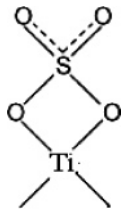

The peaks at 1622−1628 and 3372−3393 cm^{-1} are attributed to bending and stretching frequencies of water molecules occluded in the sample.[24]

Single-point surface areas of Fe(III) salt-impregnated titania catalysts calcined at 723 K are shown in Table 2. A slight decrease was observed in the surface areas of the catalysts in the case of Fe(III) ion-impregnated P25 using ferric nitrate (47 m^2/g for Ti−N5) compared to Degussa P25 (surface area = 50 m^2/g). The surface area of Fe(III) ion-impregnated P25 using ferric chloride and ferric sulfate decreased up to 43 and 15 m^2/g, respectively, with an increase in the amounts of ferric chloride and ferric sulfate. Our result is different than the result observed previously where a considerable decrease in the Brunauer−Emmett−Teller (BET) surface area was observed with an increase in the ferric nitrate concentration.[25] In the case of Degussa P25, chlorination and sulfation treatments produce a detrimental effect, decreasing the surface area values. In fact, these processes take place in this case upon crystalline TiO_2, in contrast with that prepared from the sol−gel route. Therefore, a drop in surface area is observed when the chlorination and sulfation steps take places upon the crystalline oxide.[26] Along with this, the big anionic size of sulfate (0.38 nm in hydrated form) compared to those of nitrate (0.34 nm in hydrated form) and chloride (0.181 nm) is also responsible for the higher decrease in surface area of the Ti−S series. This indicates that the surface areas of the catalysts get reduced by 3, 7, and 35 m^2/g using ferric nitrate, ferric chloride, and ferric sulfate, respectively, by using the wet impregnation method. The higher decrease in surface area using ferric sulfate of impregnated catalysts, due to the plugging of pores, would have occurred with higher sulfate loading.[27]

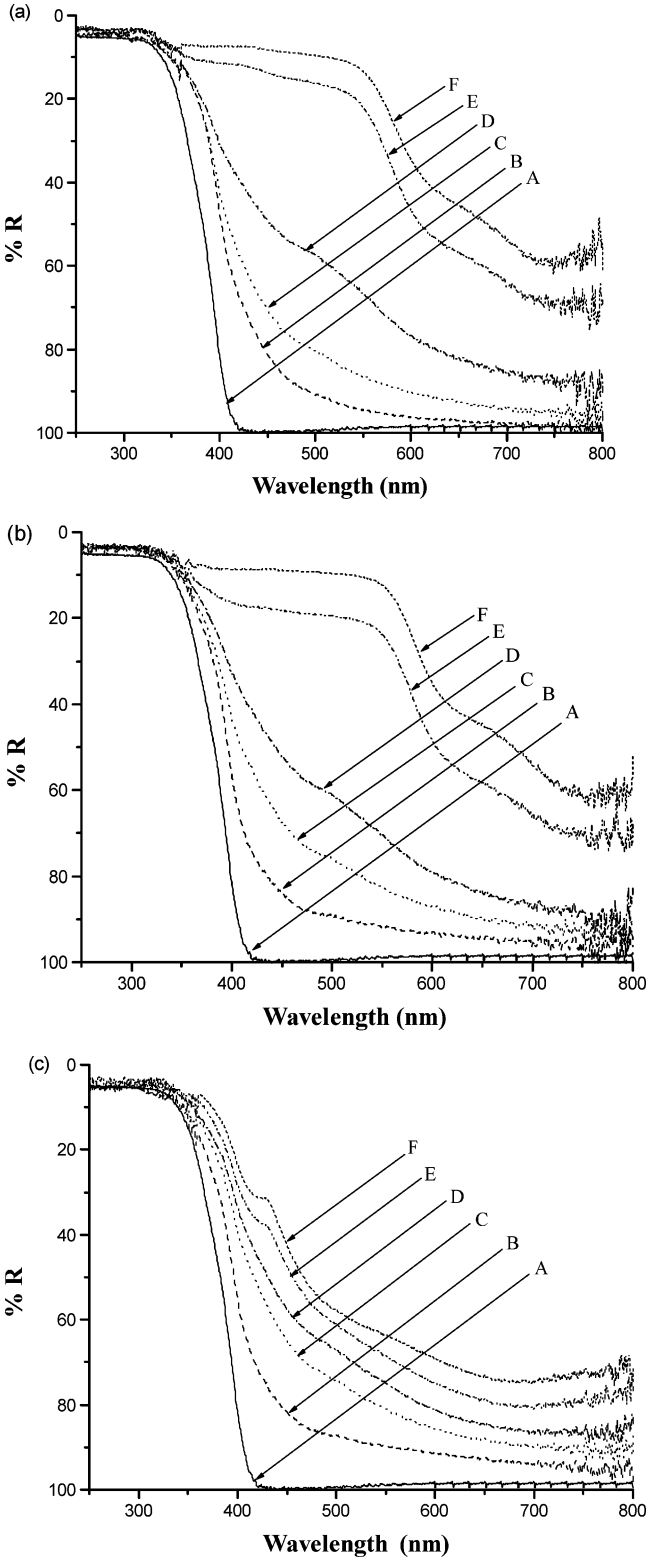

Figure 4. DRS spectra of Fe(III) salts-impregnated TiO_2 catalysts: (a) A = P25, B = Ti−N1, C = Ti−N2, D = Ti−N3, E = Ti−N4, F = Ti−N5; (b) A = P25, B = Ti−C1, C = Ti−C2, D = Ti−C3, E = Ti−C4, F = Ti−C5; and (c) A = P25, B = Ti−S1, C = Ti−S2, D = Ti−S3, E = Ti−S4, F = Ti−S5.

The diffuse reflectance spectra are shown in Figure 4. In general, the absorption of Fe(III) in octahedral symmetry is

known to appear above 430, 475, and 520 nm,[28] while the absorption of Ti^{4+} tetrahedral symmetry appears at around 375−400 nm. In the case of catalysts prepared using ferric nitrate and ferric chloride, almost all bands assigned to the Fe(III) ion octahedral symmetry were broadly seen as long tails. This meant that the Fe(III) was physically connected to the external surface of the TiO_2 anatase structure. On the other hand, in the catalysts prepared using ferric sulfate, the band slightly shifted to the left without tail broadening, reflecting that the Fe(III) ions were inserted into the pores of the TiO_2 anatase structure.[29] The absorption edge increases with the increasing amount of Fe(III) ion content along with changes on color to pale yellow or reddish−brown, while the band gap region of the TiO_2 (391 nm) remains unaffected by the presence of Fe(III) ion. At higher concentrations of Fe(III) ion, catalysts show absorption at about 584 nm with the Ti−N and Ti−C series of catalysts and at about 437 nm with the Ti−S series of the catalysts. The red shift of the absorption edge in Fe(III) ion-impregnated titania is attributed to the excitation of 3d-Fe^{3+} electrons to the TiO_2 conduction band (charge-transfer transition).[11,21,30−32]

To find the leaching of the Fe(III) ion in the catalyst during the reaction, the reaction sample was filtered and analyzed after the completion of reactions and analyzed by ICP−AAS (atomic absorption spectroscopy). The data showed the absence of any leaching of Fe(III) ion from the impregnated catalysts.

Photocatalytic Degradation of Acetophenone. The photocatalytic degradation of aqueous acetophenone solution was investigated by determining the concentrations of acetophenone after irradiation at different time intervals. The adsorption of acetophenone on TiO_2 for the first 30 min was determined without irradiation followed by photocatalytic degradation of acetophenone. In all the cases, the concentration of acetophenone after adsorption was taken as an initial concentration for calculating photocatalytic degradation. Figure 5 shows the photocatalytic disappearance of the acetophenone during the degradation in the presence of 50 mg of the catalyst in 250 mL of aqueous solution having 50 ppm initial concentration of acetophenone as a function of irradiation time under UV irradiation.

The progress of the reactions was followed by measuring the decrease in UV−visible absorption peaks corresponding to acetophenone in the 200−400 nm range in the reaction solution obtained after the filtration of photocatalyst. Typical spectra obtained after irradiation at different times are shown in Figure 6.

Photocatalytic Mechanism. The enhancement in photocatalytic activity with impregnation of the transition metal ion in the nanocrystalline TiO_2 is reported by various workers.[9,21,33−37] This enhanced activity is due to the charge trapping. The process of charge trapping in Fe(III) impregnated catalysts is as follows:

$$Ti^{4+} + e_{cb}^{-} \rightarrow Ti^{3+}$$

$$Fe^{3+} + e_{cb}^{-} \rightarrow Fe^{2+}$$

$$OH^{-} + h_{vb}^{+} \rightarrow OH^{\bullet}$$

This mechanism is supported by the visibly observed color change of the solid catalysts on Fe^{3+} reduction to Fe^{2+}. The red−brown and pale-yellow colors of the catalysts were found to change to gray. The irradiation of the semiconductor with UV light results in the formation of e^{-}/h^{+} pairs, which results in redox reactions with species present in the solution. The occurrence of these redox reactions depends on the electrochemical potential of the species and the redox level of the valence and conduction band edges of the semiconductors. The lifetimes of electrons and holes in the solution are very important, and they can be increased either by trapping an electron or a hole. Transition metal impregnation helps to decrease the recombination rate by trapping the electrons and increasing their lifetimes. Consequently, the lifetimes of free holes can be extended by moving the energy level of impreg-

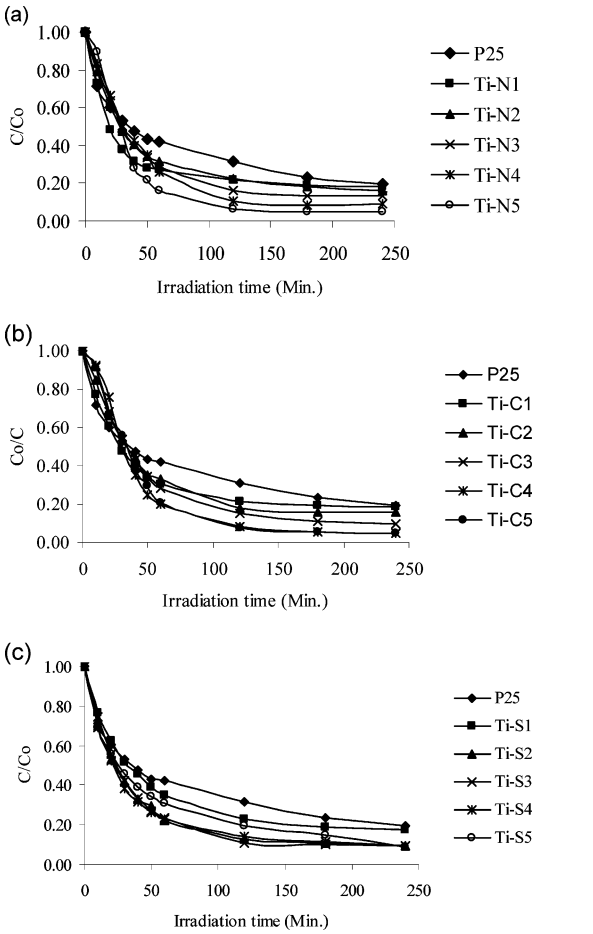

Figure 5. Photodegradation of acetophenone at different irradiation times with different Fe(III) salts-impregnated TiO_2 catalysts: (a) Ti−N series, (b) Ti−C series, and (c) Ti−S series.

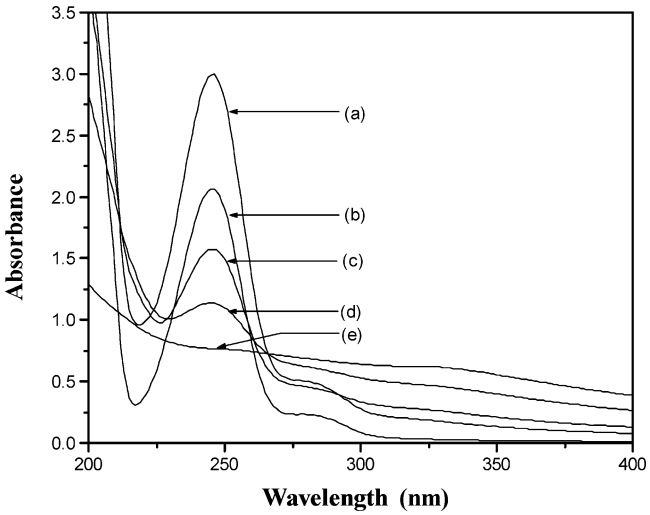

Figure 6. Typical UV spectra profile during photodegradation of acetophenone: (a) 10 min sample, (b) double-diluted 50 ppm original solution, (c) 30 min sample, (d) 60 min sample, and (e) 240 min sample.

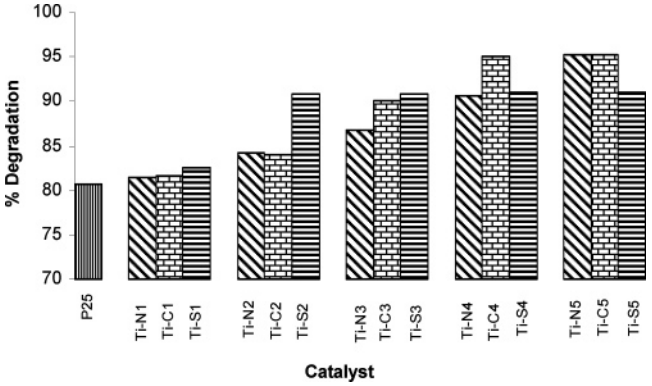

Figure 7. Photodegradation of acetophenone in aqueous suspension under UV irradiation using Fe(III)-impregnated P25 TiO_2 samples: catalyst amount = 50 mg, acetophenone concentration = 50 ppm, volume of reaction mixture = 250 mL, and reaction time = 4 h.

nated ion toward the conduction band edge, because in this case, the traps have a larger tendency to act as a shallow trap so that the holes generated by the following photons cannot recombine with already trapped electrons.[9]

The trapping of electrons makes it easy for holes to transfer onto the surface of TiO_2 and react with OH^- to form active $OH^\bullet$ radicals to participate in the acetophenone destruction.

Figure 7 shows the percentage degradation with an increase in the Fe(III) ion concentration in different catalysts after 4 h. It can be seen that the effectiveness of the catalysts increases with an increase in the Fe(III) ion content. This may be due to the charge trapping by the impregnated metal. This charge trapping stops or minimizes the charge recombination and increases the effectiveness. Thus, the anion effect is not significant as far as the final degradation is concerned.

The initial rate decreases continuously with an increase in the Fe(III) ion impregnation with the Ti−N and Ti−C series (Table 2). The initial rates observed are lower than that of pristine P25. The higher concentration of iron results in the agglomeration at the surface of the TiO_2 to form α-Fe_2O_3, as also evidenced by the X-ray diffraction data (Figure 1). This causes the reduction of catalytically active sites and electron relay sites, which would have a negative influence on the photocatalytic activity. The catalytic active sites may also be blocked by the anions.[38,39]

The scavenging feature of oxidizing radical species given by the Cl^- ion is also responsible for reducing the rate of degradation. The reactions were performed at pH = 6, and at this pH, Cl^- ion can reduce TiO_2 valence band holes forming HClO or Cl_2 as follows:[40]

$$OX^\bullet + Cl^- \rightarrow Cl^\bullet \quad \{\text{radical scavenging}\}$$

$$h_{vb}^{+} + Cl^- \rightarrow Cl^\bullet$$

$$OH^\bullet + Cl^\bullet \rightarrow HOCl$$

$$Cl^\bullet + Cl^\bullet \rightarrow Cl_2$$

NO_3^- ion may block the active sites of the catalysts. The decrease in rate was higher in the presence of NO_3^- than that of Cl^- ions. It may be because nitrate has a larger anionic size than chloride, which could block the active sites more effectively. The existence of Cl^- was confirmed by X-ray fluorescence (XRF) spectroscopy. The decreasing photoactivity in the presence of anions was observed by others with photocatalytic degradation of humic acid,[38] *para*-hydroxybenzoic acid,[41] phenol,[42] nitrobenzene,[43] and benzoic acid[44] and for the photocatalytic oxidation of organic carbon.[37]

In the case of the Ti−S series (Table 2), the initial rate was found to be lower than that of the P25 with Ti−S1, Ti−S2, and Ti−S3 catalysts but at higher impregnation of ferric sulfate, i.e., with Ti−S5 catalyst, increased rates of degradation were observed. The initial rate decrease as SO_4^{2-} ions are introduced in P25 by ferric sulfate (catalyst Ti−S1) is for the reason that the SO_4^{2-} ions are present on the surface of catalyst P25, deactivating a portion of the catalyst.[45] However, the observed rate increase with the increasing amount of SO_4^{2-} ions is explained in terms of the formation of reactive species such as $SO_4^{\bullet-}$ according to the following reaction.[38,39]

$$h_{vb}^{+} + SO_4^{2-} \rightarrow SO_4^{\bullet-}$$

The increase in the percentage degradation after 4 h may also be due to the leaching of anions from active sites of the catalysts. In the case of ferric sulfate, the sulfate ions also enhance the degradation, resulting in an increase in photocatalytic activity; however, this is not the case for ferric nitrate and ferric chloride, because such chloride ions are known as inhibitors in photocatalytic activity.

For photocatalysis, TiO_2 requires UV-light only and the presence of Fe^{3+} does not affect or only marginally affects this property. There is no visible light irradiated photocatalytic activity observed for the iron-impregnated titania samples,[25] which confirms lack of formation of e^-/h^+ pairs at these wavelengths.

The experimental kinetic data follow the first-order kinetic expression

$$\log[C_t] = -kt + \log[C_o]$$

where $[C_o]$ and $[C_t]$ represent the concentrations of the substrate in solution at time zero and time t of illumination, respectively, and k represents the apparent rate constant (min^{-1}). The values of the constant k for each reaction at every time suggest the applicability of the first-order kinetics with respect to acetophenone. The photocatalytic degradation exhibited pseudo-first-order kinetics with respect to acetophenone concentration. The rate constants were determined by linear regression of the data over the first 60 min of the reaction. The values of the average rate constants obtained are represented in Table 2. The decreasing values of average rate constants are found to decrease in the Ti−N series, while increasing values of rate constants in the Ti−S series show an increase in the rate of acetophenone degradation. The average rate constant value is almost constant for the Ti−C series, showing not much difference in rates.

Conclusions

The impregnation of Fe(III) salts on Degussa P25 TiO_2 with different anions has been found to affect the activity of the photocatalyst for the degradation of acetophenone. The metal ion impregnation inhibits the recombination of the charge species electron and holes. It results in an increase of the efficiency of catalyst, which is observed in the form of an increase in the final percentage degradation of acetophenone. The final percentage degradation increases continuously with an increase in Fe(III) ion concentration, and it was observed that anion effect is not significant in this case. On the contrary, the initial rate of degradation is reduced in the presence of the Fe(III) ion-impregnated catalyst prepared with ferric nitrate and ferric chloride. This decrease in the rate is possibly due to a

partial blockage of the active sites of the catalyst by anions. Cl^- ion can also reduce the rate of degradation by scavenging oxidizing radical species. In the case of Fe(III) ion-impregnated catalyst prepared with ferric sulfate, first the initial rate was found to decrease as SO_4^{2-} ions are introduced in P25 by ferric sulfate. This was for the reason that the SO_4^{2-} ions are present on the surface of catalyst P25 and deactivate a portion of the catalyst; however, the rate was found to increase with the increasing amount of SO_4^{2-} ions, which could be due to the formation of reactive species such as $SO_4^{\bullet-}$ radicals.

Acknowledgment

The authors are thankful to the Council of Scientific and Industrial Research, New Delhi, and Dr. P. K. Ghosh, Director of CSMCRI, for the financial assistance and support. The authors are also thankful to Dr. Pragnya Bhatt, Mr. Vinod Kumar Agarwal, Mr. A. P. Sunil, Mr. K. P. Prashanth, Mr. Renjith Pillai, and Mr. Harish D. Jirimali for analytical support.

Literature Cited

(1) Li, B.; Wang, X.; Yan, M.; Li, L. Preparation and characterization of nano-TiO_2 powder. *Mater. Chem. Phys.* **2003**, *78*, 184−188.

(2) Nagaveni, K.; Sivalingam, G.; Hegde, M. S.; Madras, G. Solar photocatalytic degradation of dyes: high activity of combustion synthesized nano TiO_2. *Appl. Catal., B* **2004**, *48*, 83−93.

(3) Irie, H.; Watanabe, Y.; Hashimoto, K. Carbon-doped Anatase TiO_2 Powders as a Visible-Light Sensitive Photocatalyst. *Chem. Lett.* **2003**, *32*, 772−773.

(4) Yang, S.; Gao, L. New Method to Prepare Nitrogen-Doped Titanium Dioxide and its Photocatalytic Activities Irradiated by Visible Light. *J. Am. Ceram. Soc*. **2004**, *87* (9), 1803−1805.

(5) Liu, H.; Gao, L. (Sulfur, Nitrogen)-Codoped Rutile-Titanium Dioxide as a Visible-Light-Activated Photocatalyst. *J. Am. Ceram. Soc*. **2004**, *87* (8), 1582−1584.

(6) Yu, J. C.; Yu, J. G.; Ho, W. K.; Jiang, Z. T.; Zhang, L. Z. Effects of F^- Doping on the Photocatalytic Activity and Microstructures of Nanocrystalline TiO_2 Powders. *Chem. Mater.* **2002**, *14*, 3808−3816.

(7) Litter, M. I. Heterogeneous photocatalysis transition metal ions in photocatalytic systems. *Appl. Catal., B* **1999**, *23*, 89−114.

(8) Brezová, V.; Blažková A.; Karpinský, L.; Grošková J.; Havlínová, B.; Jorík, V.; Čeppan, M. Phenol decomposition using Mn^+/TiO_2 photocatalysts supported by the sol−gel technique on glass fibers. *J. Photochem. Photobiol., A* **1997**, *109*, 177−183.

(9) Tayade, R. J.; Kulkarni, R. G.; Jasra, R. V. Transition Metal Ion Impregnated Mesoporous TiO_2 for Photocatalytic Degradation of Organic Contaminants in Water. *Ind. Eng. Chem. Res*. **2006**, *45*, 5231−5238.

(10) Choi, W.; Termin, A.; Hoffmann, M. R. The Role of Metal Ion Dopants in Quantum-Sized TiO_2: Correlation between Photoreactivity and Charge Carrier Recombination Dynamics. *J. Phys. Chem.* **1994**, *98*, 13669−13679.

(11) Li, X.; Yue, P.; Kutal, C. Synthesis and photocatalytic oxidation properties of iron doped titanium dioxide nanosemiconductor particles. *New J. Chem*. **2003**, *27*, 1264−1269

(12) Vamathevan, V.; Tse, H.; Amal, R.; Low, G.; McEvoy, S. Effects of Fe^{3+} and Ag^+ ions on the photocatalytic degradation of sucrose in water. *Catal. Today* **2001**, *68*, 201−208.

(13) Martin, S. T.; Herrmann, H.; Choi, W.; Hoffmann, M. Time-resolved microwave conductivity. Part 1. TiO_2 photoreactivity and size quantization. *Faraday Trans*. **1994**, *90*, 3315−3322.

(14) Spurr, R. A.; Myers, H. Quantitative Analysis of Anatase−Rutile Mixture with an X-ray Diffractometer. *Anal. Chem.* **1957**, *29* (9), 760−762.

(15) Cullity, B. D.; Stock, S. R. *Elements of X-ray Diffraction*, 3rd ed.; Prentice Hall, Inc.: Upper Saddle River, NJ, 2001.

(16) Gratzel, M. *Heterogeneous Photochemical Electron Transfer*; CRC Press: Baton Rouge, LA, 1988.

(17) Tayade, R. J.; Kulkarni, R. G.; Jasra, R. V. Photocatalytic Degradation of Aqueous Nitrobenzene by Nanocrystalline TiO_2. *Ind. Eng. Chem. Res*. **2006**, *45*, 922−927.

(18) Shah, S. I.; Li. W.; Hung, C.-P.; Jung, U.; Ni, C. Study of Nd^{3+}, Pd^{2+}, Pt^{4+}, and Fe^{3+} dopant effect on photoreactivity of TiO_2 nanoparticles. *Proc. Natl. Acad. Sci. U.S.A.* **2003**, *99*, 6482−6486.

(19) Diebold, U. The surface science of titanium dioxide. *Surf. Sci. Rep.* **2003**, *48*, 53−229.

(20) Cerius^2, v. 4.1; Accelrys, Inc.: San Diego, CA, 1999.

(21) Litter, M. I.; Navío, J. A. Photocatalytic properties of iron-doped titania semiconductors. *J. Photochem. Photobiol., A* **1996**, *98*, 171−181.

(22) Kim, E. J.; Hahn, S.-H. Microstructural changes of microemulsion-mediated TiO_2 particles during calcinations. *Mater. Lett.* **2001**, *49*, 244−249.

(23) Mishra, M. K; Tyagi, B.; Jasra, R. V. Effect of Synthetic Parameters on Structural, Textural, and Catalytic Properties of Nanocrystalline Sulfated Zirconia Prepared by Sol−Gel Technique. *Ind. Eng. Chem. Res*. **2003**, *42*, 5727−5736.

(24) Lopez, T.; Gomez, R.; Sanchez, E.; Tzompantzi, F.; Vera, L. Photocatalytic Activity in the 2,4-Dinitroaniline Decomposition over TiO_2 Sol−Gel Derived Catalysts. *J. Sol-Gel Sci. Technol.* **2001**, *22*, 99−107.

(25) Navío, J. A.; Colón, G.; Litter, M. I.; Bianco, G. N. Synthesis, characterization and photocatalytic properties of iron-doped titania semiconductors prepared from TiO_2 and iron(III) acetylacetonate. *J. Mol. Catal., A* **1996**, *106*, 267−276.

(26) Colón, G.; Hidalgo, M. C.; Navío, J. A. Photocatalytic behaviour of sulphated TiO_2 for phenol degradation. *Appl. Catal., B* **2003**, *45*, 39−50.

(27) Dalai, A. K.; Sethuraman, R.; Sai, P. Katikaneni, R.; Idem, R. O. Synthesis and Characterization of Sulfated Titania Solid Acid Catalysts. *Ind. Eng. Chem. Res.* **1998**, *37*, 3869−3878.

(28) Lee, S.-H.; Sung, M. K.; Cho, M.; Han, G. Y.; Kim, B.-W.; Yoon, K. J.; Chung, C.-H. Synthesis of TiO_2 photocatalyst thin film by solvothermal method with a small amount of water and its photocatalytic performance. *J. Photochem. Photobiol., A* **2001**, *146*, 121.

(29) Kang, M.; Choung, S.-J.; Park, J. Y. Photocatalytic performance of nanometer-sized Fe_xO_y/TiO_2 particle synthesized by hydrothermal method. *Catal. Today* **2003**, *87*, 87−97.

(30) Zhu, J.; Zheng, W.; He, B.; Zhang, J.; Anpo, M. Characterization of Fe−TiO_2 photocatalysts synthesized by hydrothermal method and their photocatalytic reactivity for photodegradation of XRG dye diluted in water. *J. Mol. Catal., A* **2004**, *216*, 35−43.

(31) Borgarello, E.; Kiwi, J.; Pelizzetti, E.; Visca, M.; Graetzel, M. Sustained water cleavage by visible light. *J. Am. Chem. Soc*. **1981**, *103*, 6324−6329.

(32) Wang, Y.; Cheng, H.; Hao, Y.; Jiming, M. A.; Li, W.; Cai, S. Preparation, characterization and photoelectrochemical behaviors of Fe-(III)-doped TiO_2 nanoparticles. *J. Mater. Sci.* **1999**, *34*, 3721−3729.

(33) Brezova, V.; Blazkova, A.; Karpinsky, L.; Groskova, J.; Havlinova, B.; Jorik, V.; Ceppan, M. Phenol decomposition using M^{n+}/TiO_2 photocatalysts supported by the sol−gel technique on glass fibers. *J. Photochem. Photobiol., A* **1997**, *109*, 177−183.

(34) Ikeda, S.; Sugiyama, N.; Pal, B.; Marci, G.; Palmisano, L.; Noguchi, H.; Uosaki, K.; Ohtani, B. Photocatalytic activity of transition-metal-loaded titanium(IV) oxide powders suspended in aqueous solutions: Correlation with electron-hole recombination kinetics. *Phys. Chem. Chem. Phys.* **2001**, *3*, 267−273.

(35) Fuerte, A.; Hernandez-Alonso, M. D.; Maria, A. J.; Martinez-Arias, A.; Fernandez-Garcia, M.; Conesa, J. C.; Soria, J. Visible light activated nanosized doped-TiO_2 photocatalysts. *Chem. Commun.* **2001**, *24*, 2718−2719.

(36) Chen, Y.-F.; Lee, C.-Y.; Yang, M.-Y.; Chiu, H.-T. The effect of calcination temperature on the crystallinity of TiO_2 nanopowders. *J. Cryst. Growth* **2003**, *247*, 363−370.

(37) Liqiang, J.; Xiaoarn, S.; Naifu, X.; Baiqi, W.; Weimain, C.; Honggang, F. The preparation and characterisation of La doped TiO_2 nanoparticles and their photocatalytic activity. *J. Solid State Chem.* **2004**, *177*, 3375−3382.

(38) Al-Rasheed, R.; Cardin, D. J.; Photocatalytic, degradation of humic acid in saline waters. Part 1. Artificial seawater: Influence of TiO_2, temperature, pH, and air-flow. *Chemosphere* **2003**, *51*, 925−933.

(39) Abdullah, M.; Gary, K. C. Low, R. W. M. Effects of common inorganic anions on rates of photocatalytic oxidation of organic carbon over illuminated titanium dioxide. *J. Phys. Chem.* **1990**, *94* (17), 6820−6825.

(40) Boxall, C.; Kelsall, G. H. Photoelectrophoresis of colloidal semiconductors. Part 1. The technique and its applications. *Faraday Trans.* **1991**, *87* (21), 3537−3545.

(41) Subramanian, V.; Pangarkar, V. G.; Beenackers, A. A. C. M. Photocatalytic degradation of *para*-hydroxybenzoic acid: Relationship between substrate adsorption and photocatalytic degradation. *Clean Prod. Process.* **2000**, *2*, 149−156.

(42) Yawalkar, A. A.; Bhatkhande, D. S.; Pangarkar, V. G.; Beenackers, A. A. C. M. Solar-assisted photochemical and photocatalytic degradation of Phenol. *J. Chem. Technol. Biotechnol.* **2001**, *76*, 363−370.

(43) Bhatkhande, D. S.; Pangarkar, V. G.; Beenackers, A. A. C. M. Photocatalytic degradation of nitrobenzene using titanium dioxide and concentrated solar radiation: Chemical effects and scaleup. *Water Res.* **2003**, *37*, 1223−1230.

(44) Ajmera, A. A.; Sawant, S. B.; Pangarkar, V. G.;. Beenackers, A. A. C. M. Solar-Assisted Photocatalytic Degradation of Benzoic Acid Using Titanium Dioxide as a Photocatalyst. *Chem. Eng. Technol*. **2002**, *25* (2), 173−180.

(45) Houas, A.; Lachheb, H.; Ksibi, M.; Elaloui, E.; Guillard, C.; Herrmann, J.-M. Photocatalytic degradation pathway of methylene blue in water. *Appl. Catal., B* **2001**, *31*, 145−157.

Received for review February 20, 2007
Revised manuscript received June 22, 2007
Accepted July 10, 2007

IE0702678